ADVANCED FUNCTIONAL MATERIALS
www.afm-journal.de

Thermo-Mechanically Stable, Liquid Metal Embedded Soft Materials for High-Temperature Applications

*Robert Herbert, Piotr Mocny, Yuqi Zhao, Ting-Chih Lin, Junbo Zhang, Michael Vinciguerra, Sunny Surprenant, Wui Yarn Daphne Chan, Swarun Kumar, Michael R. Bockstaller, Krzysztof Matyjaszewski, and Carmel Majidi**

Liquid-metal embedded elastomers (LMEEs) have been demonstrated to show a variety of excellent properties, including high toughness, dielectric constant, and thermal conductivity, with applications across soft electronics and robotics. However, within this scope of use cases, operation in extreme environments – such as high-temperature conditions – may lead to material degradation. While prior works highlight the functionality of LMEEs, there is limited insight on the thermal stability of these soft materials and how the effects of liquid metal (LM) inclusions depend on temperature. Here, the effects on thermal stability, including mechanical and electrical properties, of LMEEs are introduced. Effects are characterized for both fluoroelastomer and other elastomer-based composites at temperature exposures up to 325 °C, where it is shown that embedding LM can offer improvements in thermo-mechanical stability. Compared to elastomer like silicone rubber that has been previously used for LMEEs, a fluoroelastomer matrix offers a higher dielectric constant and significant improvement in thermo-mechanical stability without sacrificing room temperature properties, such as thermal conductivity and modulus. Fluoroelastomer-LM composites offer a promising soft, multi-functional material for high-temperature applications, which is demonstrated here with a printed, soft heat sink and an endoscopic sensor capable of wireless sensing of high temperatures.

1. Introduction

Liquid metal elastomer (LMEE) composites are an emerging set of materials in which thermal and electrical properties can be tailored without affecting the mechanical properties of the polymer matrix, which is distinct from the use of rigid fillers.[1–7] A variety of improvements can be made to the polymer matrix with the use of liquid metal (LM) inclusions, including toughness, dielectric constant, thermal conductivity, self-healing, and electrical conductivity, without stiffening or weakening the soft material matrix.[2,7–16] Eutectic gallium indium alloy (EGaIn) is frequently used as a LM filler, owing to its low toxicity, high thermal conductivity, and high electrical conductivity.[2,17–23] Commonly used polymer matrix materials include polydimethylsiloxane (PDMS) materials, such as Sylgard (Sylgard 184, Dow Corning Corp.) and Ecoflex (Ecoflex 30, Smooth-On), and polystyrene-block-polyisoprene-block-polystyrene styrene (SIS), and these

R. Herbert, M. Vinciguerra, C. Majidi
Department of Mechanical Engineering
Carnegie Mellon University
Pittsburgh, PA 15213, USA
E-mail: cmajidi@andrew.cmu.edu

P. Mocny, T.-C. Lin, K. Matyjaszewski
Department of Chemistry
Carnegie Mellon University
Pittsburgh, PA 15213, USA

Y. Zhao, M. R. Bockstaller
Department of Materials Science and Engineering
Carnegie Mellon University
Pittsburgh, PA 15213, USA

J. Zhang, S. Kumar
Department of Electrical and Computer Engineering
Carnegie Mellon University
Pittsburgh, PA 15213, USA

S. Surprenant, W. Y. D. Chan
Department of Chemical Engineering
Carnegie Mellon University
Pittsburgh, PA 15213, USA

The ORCID identification number(s) for the author(s) of this article can be found under https://doi.org/10.1002/adfm.202309725

DOI: 10.1002/adfm.202309725

composites have been extensively studied in prior works.[11,15,24–33] However, there remains a limited understanding of the effect of LM filler on the thermal stability of materials. Such insights are especially important for applications that demand high-temperature operation or exposure, including thermal management or sensing and actuation in extreme environments.[34–36] Applications may include aerospace and in-space systems, where materials are exposed to wide temperature fluctuations. Soft, thermally stable materials may be applied for space-grade soft sensors, flexible thermal dissipation devices, and rubbery interfaces for modular robotics. In particular, in-space additive manufacturing is of growing interest for on-demand fabrication and repairs, and the deposition of tough, soft materials for repairs may be a promising direction. Few prior works have investigated the thermal stability and temperature-dependent effects of LM filler on elastomer composites, including a study on thermal conductivity dependence on cyclic temperature of EGaIn and copper particle composites.[37] Additionally, the stability of thermal conductivity of an LM-aramid nanofiber composite was studied.[38] For LMEEs, the effect of LM for low-temperature applications was studied.[26] Overall, more needs to be understood about the thermal stability of LM composites at high temperatures and how it may be influenced by the choice of elastomer matrix material. In particular, the thermomechanical stability and maintenance of the rubbery mechanics of these soft composites at high temperatures have not been demonstrated.

In contrast to the more commonly used elastomers, fluoroelastomers (FKM) offer an advantageous matrix material to embed LM droplets. Common FKMs include poly(vinylidene difluoride) (PVDF) and its copolymers with hexafluoropropylene and vinylidene fluoride (PVDF-HFP).[24,39–42] Additionally, other PVDF copolymers include piezoelectrics and ferroelectrics, such as P(VDF-TrFE-CTFE). Owing to the high thermal stability, mechanical durability, and chemical resistance of FKMs, LM composites with FKMs may realize new applications of soft materials in high-temperature or extreme environment settings. PVDF-HFP materials, such as Viton (Chemours), offer a wide working temperature range up to 250 °C while maintaining soft mechanics. Importantly, the embedding of LM droplets in FKM may offer multifunctional materials suitable for high temperatures without significantly affecting the excellent mechanical properties of FKMs. Several studies included the use of an FKM matrix to embed nanomaterials, including a study reporting the high dielectric constant of an LM-FKM composite, but the effect on the thermal stability and suitability for high-temperature application of the composite was not characterized.[39,43–48] One prior work investigated improving the thermal stability of FKM with the use of rigid nanoparticles.[43] Collectively, there is a limited understanding regarding the impact of LM droplets on the thermal stability of a soft composite and the potential of an LM-FKM composite for high-temperature applications.

Here, we address this gap in knowledge of LM composites by characterizing the thermal stability of the mechanical and electrical properties after exposure to high temperatures. This exploratory work aims to provide a comprehensive introduction into the effect of LM on the thermal stability of soft composites, with a focus on LM-FKM properties. This includes comparison across both LM-FKM (**Figure 1**a) and conventional LM-elastomer (Figure 1b) composites at 0%, 20%, and 40% volume fill fractions (φ) of LM. Figure 1 shows a comparison between composites using Viton as an FKM matrix and Ecoflex as a conventional elastomer matrix. Composites were exposed to temperatures up to 325 °C to study the effects of LM on the temperature dependence of modulus, ultimate strain, and dielectric properties. Thermomechanical stability is evaluated to highlight the effects of matrix material and LM volume fill fraction. As shown in Figure 1c–d, LM-Viton composites offer a distinct improvement in thermomechanical stability, with the effect of LM being broadly beneficial to thermomechanical stability, although the results are variable based on the matrix material. The effect of dielectric and thermal properties (Figure 1e–h) were compared, where a Viton matrix provides an increased baseline for dielectric constant (ϵ_r) and a similar thermal conductivity (k). This study of the thermal stability of LM composites broadens the view on the effect of LM, and the selection of an FKM matrix enables the application of soft electronics and robotics in high-temperature environments. LM-FKM composites are shown to be compatible with 3D printing (Figure 1i), which is applied to fabricate a soft heat sink (Figure 1j). The use of thermally stable LM-FKM composites is highlighted in an endoscopic sensor for wireless monitoring of high temperatures (Figure 1k). Collectively, characterizing thermal stability and the effect of an FKM matrix for LM composites provides a broadened understanding of the effect of LM droplets. While commonly used LM composites degrade at elevated temperatures, thermally stable LM composites could lead to multifunctional materials for soft robotics operating in extreme environments, including aerospace, chemical, or high-temperature settings.

2. Results and Discussion

2.1. Synthesis of LM-FKM Composites

LM-FKM composites and LMEEs with more conventional choices of elastomer matrix material were fabricated with a range of different matrix materials in order to highlight the effects of LM on composite performance and on thermal stability. **Figure 2**a illustrates the fabrication process for LM-FKM composites. FKM materials include Viton A401C (PVDF-HFP), Daikin G801EL (PVDF-HFP), PVDF-HFP (Sigma–Aldrich), PVDF, PVDF-CTFE, and PVDF-TrFe. FKM was mixed in solvent (dimethylformamide; DMF) at a constant 22.5% mass ratio until a uniform solution was achieved. EGaIn was added to the solution and mixed in a planetary mixer. EGaIn was added in 0%, 20%, and 40% volume fractions with respect to polymer volume. The LM-FKM solutions can be cast and dried to produce a thin composite film. It should be noted that the ratio of solvent to FKM can be adjusted to produce a higher viscosity ink compatible with 3D printing. Elastomer-based composites were also created with PDMS materials of Sylgard 184 and Ecoflex 30, a urethane rubber (Vytaflex 30, Smooth-On), and SIS, which were diluted with solvent (toluene) for mixing with EGaIn.

Figure 2b shows optical images of Viton and LM-Viton, where a darkening color is observed as LM is added. Microscopy images show the dispersion and size of LM droplets. In this work, while a constant 22.5% mass ratio of solvent to FKM was maintained across all tested materials, the resulting viscosities of FKM solutions were varied. As a result, the dispersion and structure of

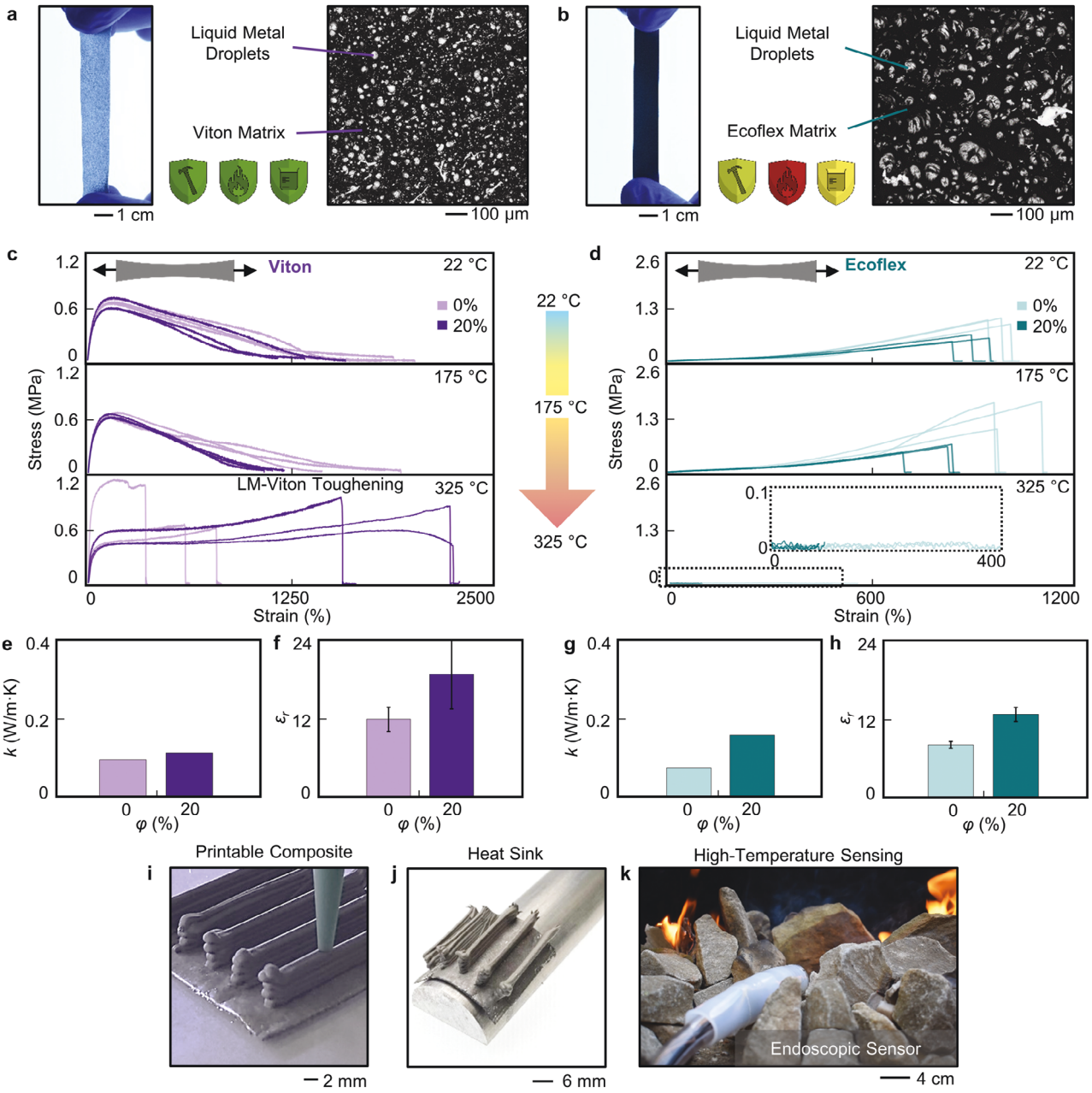

Figure 1. Comparison of LM-Viton and conventional LM-Ecoflex composites for high thermo-mechanical stability. a) Image of a stretched LM-FKM composite using Viton. SEM image of an unstrained composite shows the dispersion of LM droplets. b) Image of a stretched conventional LM-elastomer composite using Ecoflex with SEM image of embedded LM in an unstrained state. Viton offers advantages across mechanical, thermal, and chemical stabilities. c,d) Stress-strain curves of c) LM-Viton and d) LM-Ecoflex composites after being exposed to (top) room temperature, (middle) 175 °C, and (bottom) 325 °C for 10 min. An Viton matrix offers heightened stability while elastomer matrix composites show mechanical degradation. e) Dielectric constant and f) thermal conductivity of LM-Viton composite at 0% and 20% volume fraction. g) Dielectric constant of LM-Ecoflex composite is lower than that achieved with Viton as the matrix material, while h) thermal conductivity is in a similar range as FKM-LM composites. i) Photo of printing of an LM-FKM composite. j) Image of a printed heat sink for thermal management. k) Image of a temperature-sensing endoscope consisting of FKM-based materials.

LM droplets within the composites varied between matrix materials (Figure 2c; Figure S1, Supporting Information). In general, LM droplet size diameters for composite films presented in this study were between 50–100 µm. While this work compares the thermal stability of composites within this range of LM droplet sizes, future work will include tuning the LM droplet size for a given matrix material to understand how droplet size affects thermal stability. Thermal stability may depend on droplet sizes as previous works have shown effects on a variety of material properties.[7,24,26,48]

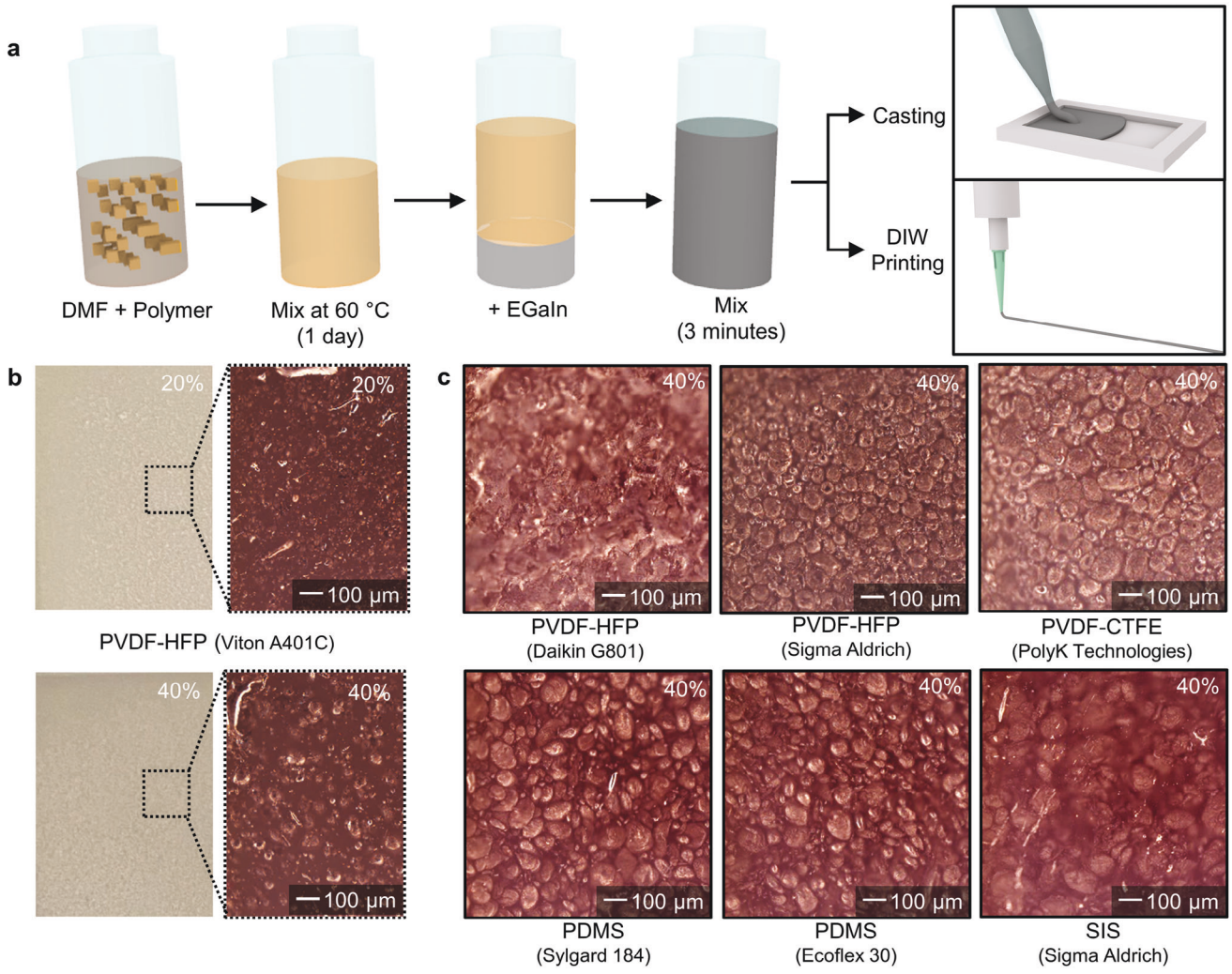

Figure 2. Overview of fabrication process and microstructures for LM-FKM composites. a) Schematic of fabrication steps involving mixing of FKM with solvent and adding EGaIn before mixing. Solutions can be created for casting or printing procedures. b) Images of LM-Viton composites of 0% (left), 20% (middle), and 40% (right) volume fractions. Optical images show the dispersion of LM droplets. c) Optical images of LM-FKM composites and LMEEs with conventional elastomer matrix with 40% volume fill fraction of LM.

2.2. Thermo-Mechanical Characterization

Thermogravimetric analysis (TGA) is a commonly used technique to evaluate the thermal stability of polymers, where the mass of a polymer is measured with increasing temperature. Mass may change due to decomposition and vaporization, among other reactions, as temperature increases. Here, TGA is performed with composites of 0% and 40% volume fractions of LM to understand the effect of LM on the thermal stability of FKMs and elastomer composites. **Figure 3**a,b shows the remaining mass of each composite as the temperature was increased up to 800 °C (additional materials in Figure S2, Supporting Information). Without the addition of LM, FKMs showed increased thermal stability in comparison to the conventional elastomers of Sylgard, Ecoflex, Vytaflex, and SIS. A 5% mass loss occurred at 349 and 343 °C for Sylgard and Ecoflex, and at 270 and 386 °C for Vytaflex and SIS. For comparison, Viton, Daikin, and PVDF-HFP showed a 5% mass loss at 415, 407, and 435 °C, respectively. With LM added to the polymer material, only minor changes in these mass losses and temperatures were observed. While the addition of LM droplets decreased the total mass lost over the temperature range, the remaining mass at 800 °C compares well with the mass of EGaIn added in each composite. These results indicate the embedding of LM droplets does not interfere with the thermal stability of the polymer matrix materials, which indicates the potential to embed LM in thermally stable materials to offer high-temperature, multifunctional composites.

While TGA offers a measure of thermal stability, it does not provide insight into whether the material is mechanically degrading at elevated temperatures. To provide further insight, thermo-mechanical responses were evaluated to determine the effects of LM inclusions on the ability of the composite to maintain a soft, rubber-like form after exposure to high temperatures. Tensile testing was performed on LM-composites after exposing the material to 100, 175, 250, and 325 °C for 10 min and then compared to samples exposed to only room temperature. All materials were

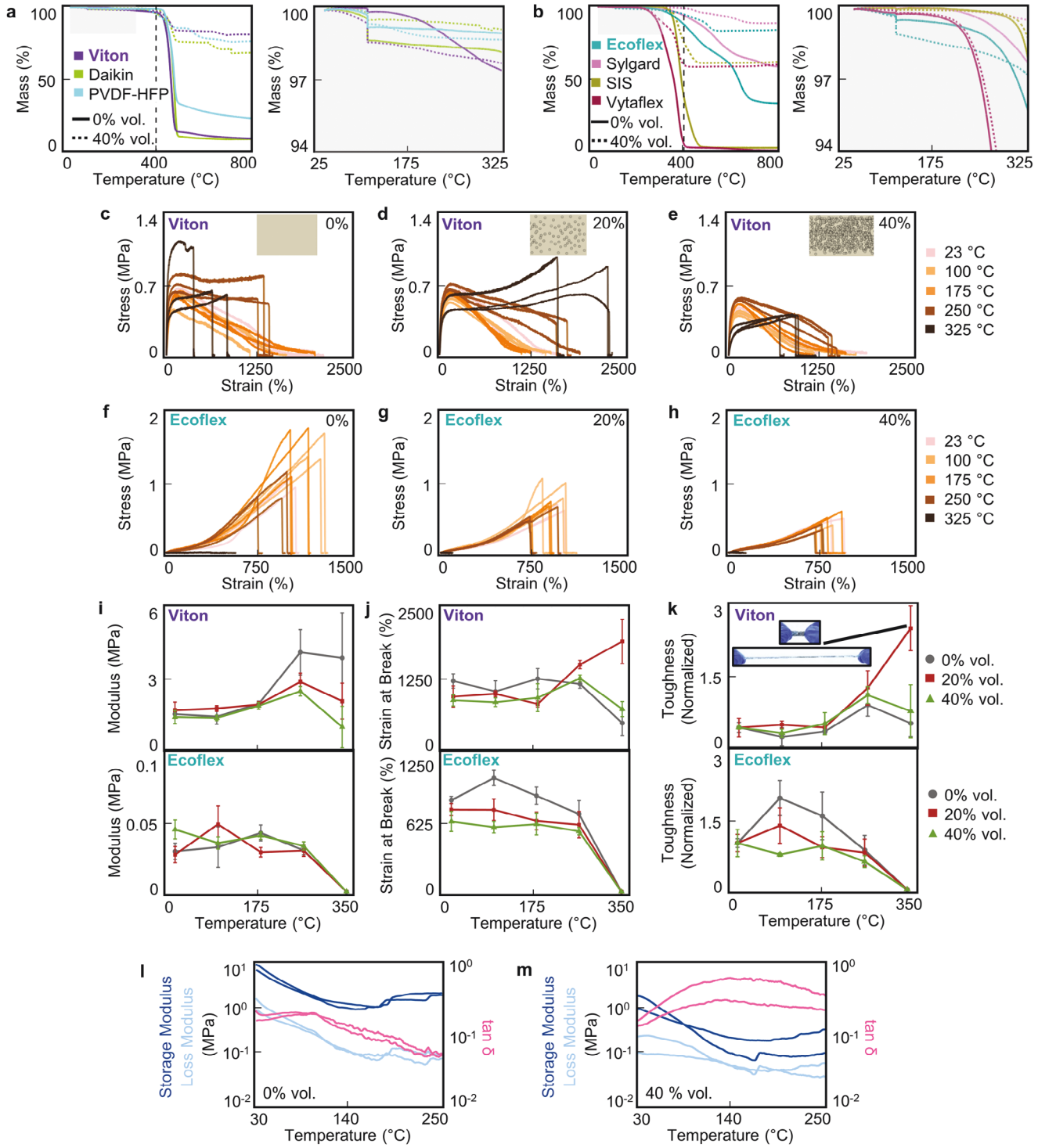

Figure 3. Thermo-mechanical evaluation of LM-FKM and conventional LM-elastomer composites. a,b) TGA curves of a) FKM-based and b) conventional elastomer-based LM composites at 0% and 40% volume fill fraction of LM. Enlarged views show a temperature range from room temperature to 325 °C. c–e) Stress-strain curves for Viton composites after exposure to different temperatures for d) Viton only, e) 20% volume fill fraction of LM, and f) 40% volume fill fraction of LM. f–h) Stress–strain curves for Ecoflex composites after exposure to different temperatures for d) Ecoflex only, e) 20% volume fill fraction of LM, and f) 40% volume fill fraction of LM. i–k) Comparison of (i) modulus, (j) strain at break, and (k) toughness after exposure to temperature for (top) Viton and (bottom) Ecoflex composites. l–m) Storage modulus, loss modulus, and damping ratio of l) Viton and m) LM-Viton (40% volume fraction of LM) across the temperature range.

cooled down to room temperature before testing. A comparative set of stress-strain curves is shown in Figure 3c–h for Viton and Ecoflex composites. Data from these stress-strain curves were further analyzed to estimate modulus, strain at break, and toughness (Figure 3i–k) for Viton (top) and Ecoflex (bottom). Modulus, strain at break, and toughness for additional materials are reported in Figures S3 and S4 (Supporting Information). Overall, LM-FKM composites showed moderate mechanical changes while conventional elastomers showed varying degrees of degradation. Figure 3c–e shows a set of stress–strain curves during tensile stretching after exposure to different temperatures for Viton. As shown in Figure 3c–e, a prominent change in stress–strain responses, including a change from strain-softening to strain hardening characteristics, was observed when the Viton composites were heated over 250 °C, which may be a result of a post-curing effect. In addition to these changes, a 20% volume fill fraction appeared to moderately toughen the Viton composite at higher temperatures. Additional sets of samples confirmed toughening effects at 325 °C for Viton with 20% volume fill fraction of LM (Figure S5, Supporting Information). Viton-based composites showed a moderate increase in modulus from its room temperature modulus of 1.4 MPa as temperature increased (Figure 3i). As shown in Figure 3j (top), Viton composites also showed a consistent strain at break of around 1000% up to 250°C, prior to a change at 325°C. At 325°C, a 20% volume fill fraction of LM is observed to increase the maximum elongation of the material and enables stretching up to 2000% strain (Video S1, Supporting Information). Although the LM-Viton composite formed bubbles upon heating at 325 °C (Figure S6, Supporting Information), the LM droplets toughened the material and enabled higher elongations, similar to a previous report on the toughening of LM-elastomer composites.[10] Figure 3k (top) quantifies the change in toughness for Viton calculated from stress–strain curves and normalized to each composite's room temperature value. The effect of LM appears to vary depending on matrix material, but for Viton composites, the addition of LM provided an increase in stability at higher temperatures. Specifically, at a 20% fill fraction of LM, LM-Viton composites showed nearly a 3x higher toughness at 325 °C than at room temperature. This improvement in toughness may share similarities in mechanism with a previous report where LM droplets enhanced the fracture toughness of elastomers.[10] Additionally, a post-curing effect may also influence the toughness of all Viton composites, as the selected Viton material can include a post-curing step of heating at 232 °C for 24 h. However, as previously mentioned, the thin rubber films that were tested would form bubbles on the surface when heated above 250 °C (Figure S6, Supporting Information). These bubbles are visually observed as regions of lighter color and become more visually apparent when stretched. It has been previously reported that the presence of LM inclusions in soft materials improve the resistance of to fracture when strained.[10] Additionally, the formation of bubbles may lead to a foam-like composite with LM inclusions. Previous work on polymeric foams have shown that embedding voids or bubbles can improve toughness, which may have a similar effect as the bubbles created here in the LM-Viton composite.[49–51] The toughness of polymeric foams has also been shown to improve with the addition of micro-fillers, such as milled carbon fiber, which enables a crack deflection mechanism that has similarly been observed for LM composites. [10,52] Overall, changes in the Viton matrix, formation of a foam-like composite, and crack deflection from LM inclusions may contribute to the increased toughness. Since the LM-Viton composites with a 40% fill fraction of LM do not show the same improvement in toughness as the 20% fill fraction composites, there may exist an optimal balance for thermo-mechanical stability and suggests degradation of matrix material may play a more pronounced role when there is less matrix material to hold the composite together.

Unlike Viton, Daikin showed a more consistent modulus and strain at break (Figure S3a,b, Supporting Information). Daikin-based composites displayed less than a 20% change in modulus with temperature, starting with a room temperature modulus of 1.2 MPa. For elongation, LM-Daikin composites offered stability up to 250 °C with elongation around 200%, prior to a decrease at 350 °C. A more consistent stress–strain curve compared to Viton was observed across all temperatures and displays stable properties until 325 °C, without any notable toughening effect (Figure S4, Supporting Information). In terms of toughness, LM-Daikin showed a minor improvement with the addition of LM at 40% volume fill fraction, where a 24% reduction in toughness occurred for Daikin only compared to 4% reduction for the LM-Daikin composite at 250 °C. Overall, both FKM materials of Viton and Daikin demonstrate thermally stable mechanics up to 325 °C with Viton demonstrating a clear improvement in toughness with the addition of LM. The difference in results may arise from the Viton being an incorporated cure polymer whereas Daikin is not.

For comparison to FKM-based composites, thermo-mechanical responses of LM composites using conventional elastomers were tested. Stress–strain curves of Ecoflex composites show degradation after exposure to 325 °C (Figure 3f–h). As shown in Figure 3i,j, Ecoflex composites (bottom) maintained a consistent modulus and failure strain up to 250 °C before severe degradation at 325 °C. Ecoflex composites maintained a stretchability over 600% and a modulus ≈40 kPa up to 250 °C, but became gel-like with no measurable modulus or failure strain after exposure to 325 °C. The addition of LM droplets does not affect this weakening as the matrix material is severely degraded. However, up to 250 °C, LM inclusions effectively enhance the thermal stability of Ecoflex at the cost of reducing maximum strain near room temperature. Modulus and strain at break were more consistent from room temperature to 250 °C for Ecoflex composites with 20% and 40% fill fractions in comparison to 0% fill fraction. Unlike the FKM composites, Ecoflex-based composites did not demonstrate any toughening effect (Figure 3k; bottom).

In addition to Ecoflex, Sylgard – a less stretchable silicone matrix – was tested. Sylgard composites showed a slight decrease in room temperature modulus from 1.4 to 0.5 MPa with the addition of LM as expected from Eshelby theory and previous works (Figure S3c-d, Supporting Information).[24,53] Results indicate the presence of LM droplets in Sylgard enables a more consistent maximum elongation and stress–strain response up to 250 °C compared to Sylgard without LM droplets, which is similar to the effect seen in Ecoflex composites (Figure S8, Supporting Information). As was observed for Ecoflex, this effective improvement in thermal stability is provided at the cost of a lower modulus and strain at break near room temperature. Sylgard shows a decrease in maximum elongation from 210% to 140% while LM-Sylgard

in 20% fill fraction shows a change from 133% to 104%. While Ecoflex composites became gel-like after exposure to 325 °C, Sylgard composites maintained a consistent modulus but became brittle and failed at lower strain. Similar to Daikin, a minor toughening effect is observed for Sylgard, where toughness changes after exposure to 250 °C improved from a 39% loss to a 25% loss to a 33% gain as LM volume fill fraction was varied from 0%, 20%, and 40% (Figure S4, Supporting Information).

In addition to these FKMs and silicone elastomers, SIS and urethane composites were characterized. Vytaflex – a urethane rubber – demonstrated the lowest thermo-mechanical stability. After exposure to 175 °C, Vytaflex composites showed a decrease in modulus from 0.35 to 0.07 MPa, with a decrease in elongation from 1000% to less than 100% (Figure S3e,f, Supporting Information). Moreover, the composites could not be tested after exposure to 250 °C or 325 °C due to severe degradation and cracking of the composites, and the stress–strain curves highlight the instabilities at temperatures as low as 175 °C (Figure S9, Supporting Information). Similarly, SIS-based composites show poor thermo-mechanical stability, with decreases in modulus and strain at break with increasing temperature (Figure S3g,h, Supporting Information). While SIS materials offered extremely high elongation at room temperature, such as with the LM-SIS composites studied here that can stretch up to 2500% strain, max elongation dropped by more than 50% after exposure to 175 °C (Figure S10, Supporting Information).[58] After exposure to 325 °C, SIS, with and without LM, becomes gel-like and could not be tested. The poor thermo-mechanical stability of Vytaflex and SIS correlates well with the low thermal stability previously observed by TGA.

In addition to these soft FKM and conventional elastomer composites, the stiffer composites of PVDF-HFP with and without LM were evaluated at room temperature and at 325 °C, which showed no significant changes in modulus. A 20% volume fill fraction of LM showed a toughening effect at room temperature (Figure S11, Supporting Information).

While the above thermo-mechanical characterizations investigate how the mechanics of LM composites change after exposure to temperatures, it does not observe mechanics during temperature exposure. Thus, dynamic mechanical analysis (DMA) was also performed to characterize thermo-mechanical stability and characterize LM-FKM mechanics while exposed to elevated temperatures. Room temperature testing was first completed and compared well with the observed trends discussed above for LM composites where only minor changes in modulus were observed with the addition of LM at a 40% volume fill fraction (Figures S12 and S13, Supporting Information).

Since LM-Viton composites demonstrated the best thermo-mechanical responses after exposure to temperature, it was selected to also be characterized during exposure to temperature. Storage modulus and loss modulus were measured at room temperature, and adding LM resulted in a decrease in both values, although there is higher variability observed in Viton samples without LM (Figure S12g,h, Supporting Information). Storage modulus, loss modulus, and damping factor (tan δ) were then measured across a temperature range from room temperature to 250 °C (Figure 3l) and LM-Viton (Figure 3m) at a 40% volume fill fraction. The addition of LM droplets showed a decrease in storage modulus at all temperatures, and a decrease in loss modulus at temperatures below 140 °C. Loss moduli become similar above 140 °C, as the LM droplets decrease the relative change in loss modulus with temperature. The damping factor of Viton and LM-Viton was similar near room temperature, but the addition of LM droplets showed a higher damping factor as temperature increased. Collectively, thermo-mechanical characterizations highlight the advantage of using FKMs as a matrix material and the effect of LM on thermal stability after exposure to high temperatures. Specifically, LM-Viton offered an improvement in toughness after exposure to high temperatures, which is distinct from the degradation observed in LM composites based on conventional elastomers.

2.3. Thermal and Electrical Characterization

While thermo-mechanical results indicate the benefit of LM-FKMs, LM inclusions have also been previously reported to increase the thermal conductivity of elastomers.[2] Here, the thermal conductivity of FKMs is characterized. **Figure 4**a shows the thermal resistance of Viton-based composites, where increasing the volume of LM decreases thermal resistance (additional FKM materials in Figure S14, Supporting Information). Thermal conductivity for Viton and Daikin at 0%, 20%, and 40% volume fill fractions of LM are summarized in Figure 4b at room temperature. Viton shows an improvement in thermal conductivity from 0.18 to 0.31 W m^{-1} K^{-1} with the addition of 40% volume fill fraction LM.

In addition to enhancing the thermal conductivity of composites, LM also enables an increase in dielectric constants, which can be applied in dielectric elastomer actuators.[24,55,56] However, prior reports have not investigated if the effect of LM on dielectrics is influenced by temperature. First, room temperature dielectric properties were evaluated and compared between FKM and elastomer composites. Figure 4c compares the dielectric constant at room temperature at different volume fill fractions of LM in a range of FKMs and elastomers. All materials showed an increase in dielectric constant with increasing LM content, and values of Sylgard, Ecoflex, and Vytaflex composites compared well with prior studies.[9,24] Notably, using FKM as a matrix material can offer a higher dielectric constant owing to the higher initial dielectric constants of FKMs. Viton showed an increase from 10.4 to 20.2 with the addition of 40% LM. PVDF-CTFE-TrFE, a ferroelectric material, showed dielectric constants of 31.5, 37.5, and 41.5 with the addition of LM at 0%, 20%, and 40% volume fractions. Dissipation factor, which is a measure of power loss in the dielectric, were also studied at room temperature. Dissipations factors are of interest as a low factor indicates reliable electrostatic energy storage and is preferred for dielectric elastomer actuators to prevent unwanted energy dissipation and heating.[24,56] Dissipation factors are summarized in Figure 4d and generally show values below 0.05, besides the ferroelectric material of PVDF-CTFE-TrFE. In addition to measuring dielectric properties at room temperature, changes in dielectric properties were evaluated after exposure to high temperatures. Materials were exposed to 100, 175, 250, and 325 °C for 10 min each and then properties were measured after cooling to room temperature. Figure 4e shows changes in capacitance with temperature for Viton-based composites (top) and Ecoflex-based composites

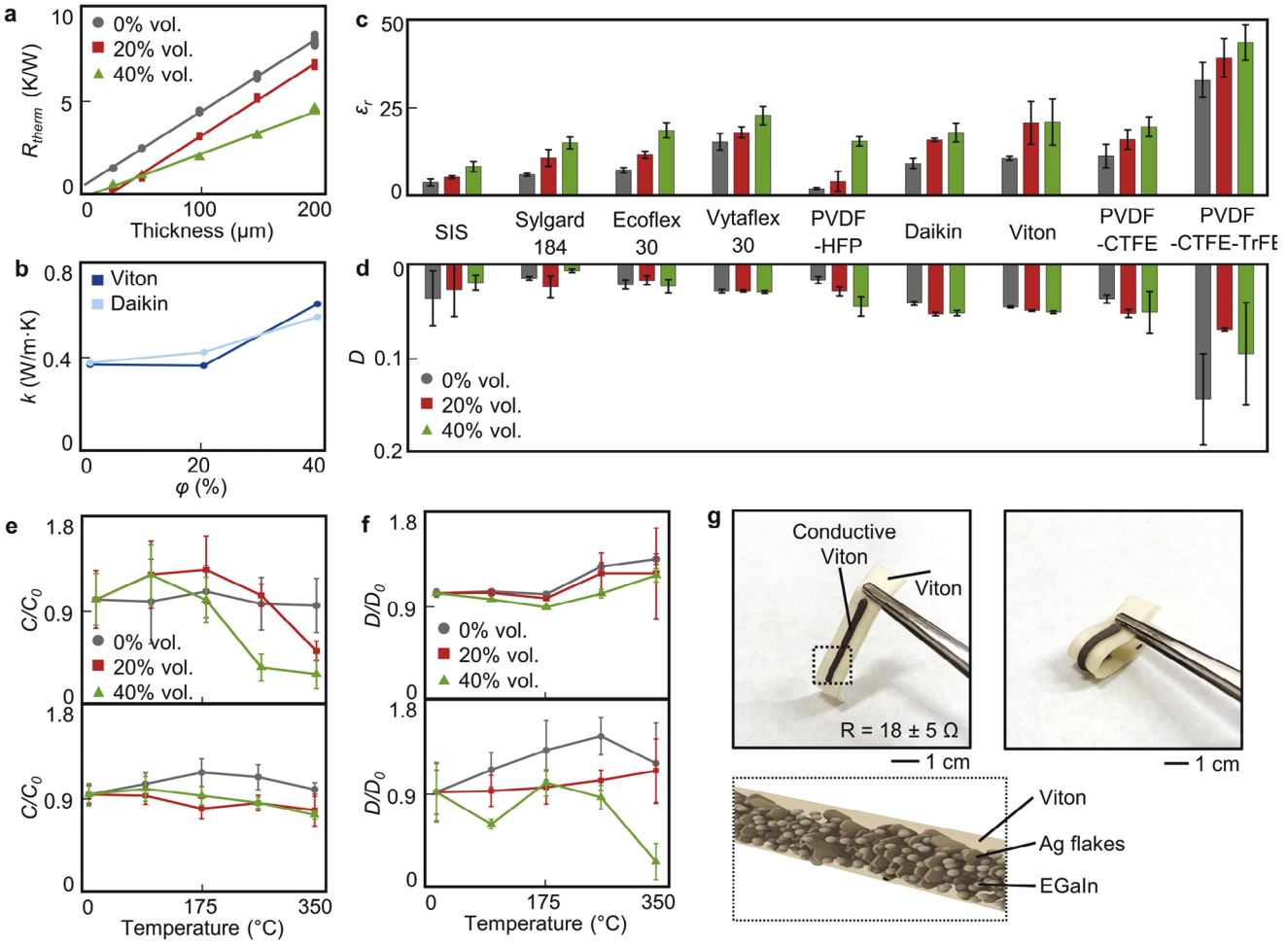

Figure 4. Thermal conductivity and electrical characterization of LM-FKM and LM-elastomer composites. a) Thermal resistance of Viton composites at various material thicknesses. b) Thermal conductivity of LM-FKM composites at different volume fill fractions of LM. c) Dielectric constant and d) dissipation factor of LM-composites for a variety of FKM and elastomer matrix materials. e,f) Thermal stability of e) measured capacitance and f) dissipation factor after exposure to temperatures for Viton (top) and Ecoflex (bottom) dielectric material. Values were normalized to room temperature values. g) FKM material embedded with LM and Ag flakes for an electrically conductive composite with high flexibility.

(bottom) while Figure 4f shows corresponding changes in dissipation factor. Here, the addition of LM in Viton demonstrates an effect on capacitance at high temperatures (250 and 325°C) while Ecoflex shows a more consistent capacitance. This difference may arise from the different mechanical responses of the composites, where Viton may be prone to bubbling while Ecoflex becomes a tacky gel. Similar to Viton, Daikin-based composites showed increased changes at higher temperatures (Figure S15, Supporting Information). Elastomer composites using Sylgard and Ecoflex demonstrated similar trends. Notably, after testing at exposures to 325°C, LM-Sylgard composites were fractured due to their mechanical instability when the steel substrate was handled.

In addition to dielectric materials, LM may also be employed for electrically conductive composites.[11,29,48] Recently, mixtures of LM and Ag flakes in SIS have been reported to enable highly stretchable conductors.[11,29] While composites embedding only LM can be activated or sintered to become electrically conductive, the additon of Ag flakes enables sinter-free fabrication. To demonstrate the potential for FKM-based electrical conductors, Viton-based composites were filled with LM and Ag flakes to create electrically conductive FKM materials following recipes of previous LM-Ag-SIS composites.[11,29] As shown in Figure 4g, a composite of LM-Ag-Viton was deposited and dried to form an electrical conductor. The electrically conductive Viton material maintained high flexibility and stretchability, as imaged in Figure 4g. By enabling FKM-based insulating, dielectric, and conductive materials, soft electronic devices fully reliant on FKM matrix materials could be achieved for high temperature or extreme environment applications where the stability of FKMs is demanded. Interestingly, the electrically conductive mixing ratios of Viton appear to not be extendable to Daikin and reasoning for this outcome is unclear, thus future work will be to develop fabrication procedures for LM-based electrically conductive FKM and to characterize the thermal stability of the conductors. While the difference in viscosity of the polymer solutions of SIS, Viton, and Daikin may cause differences in filler dispersion, future work, such as tailoring the type and quantity of Ag flake, is necessary to better comment on electrically conductive FKM composites.

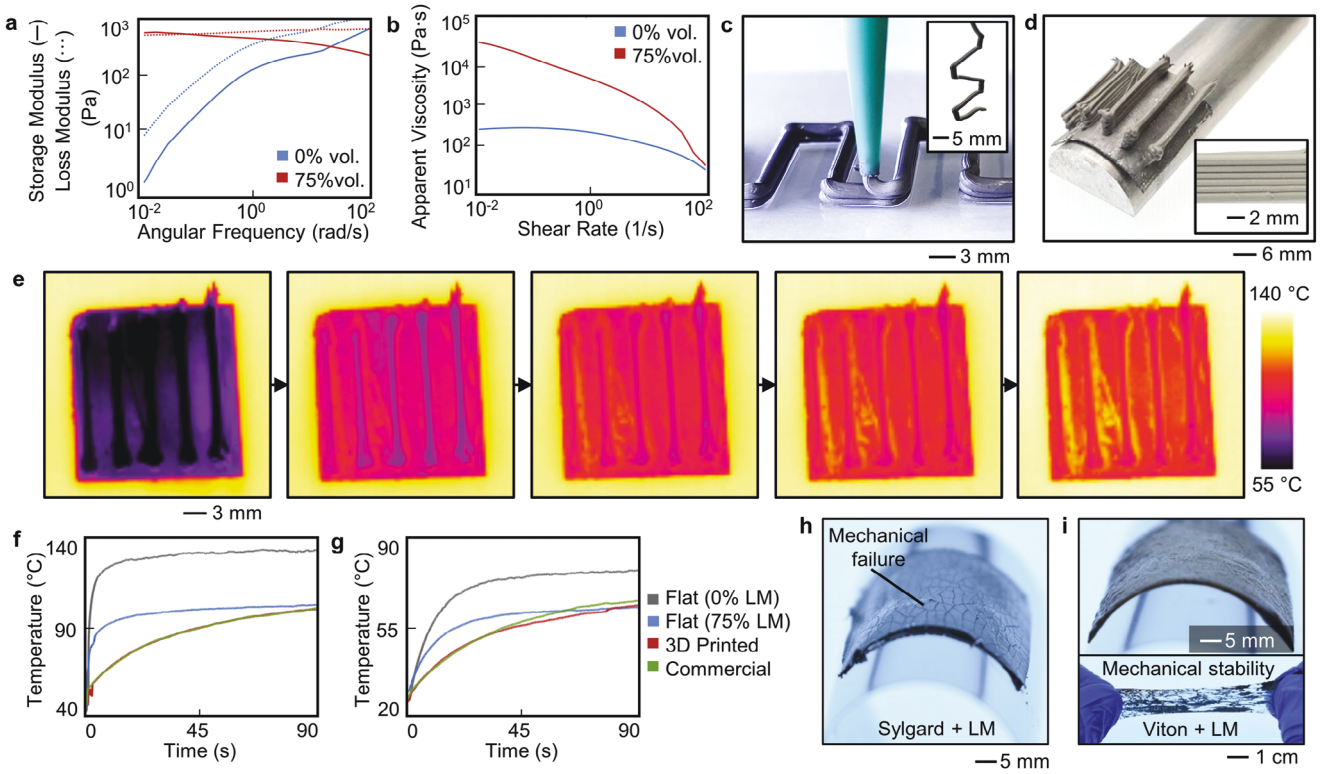

Figure 5. Printing of LM-FKM composites and application for creating a soft heat sink. a) Storage and loss moduli and b) apparent viscosity of Daikin and LM-Daikin inks. c) Photo of printing a LM-FKM multilayered trace. Inset photo shows printed pattern held in hand. d) Printed heat sink conformally wrapped on a curved surface. Inset photo shows side-view of a heat fin printed with multiple layers. e) Infrared images of a flat heat sink and a 3D printed heat sink being heated to 135°C. f,g) Average temperature measured from heat sinks heated to f) 135 °C and g) 75 °C. h) Image of LM-Sylgard cracking after exposure to 325 °C followed by mechanical bending. i) Image of LM-Viton after exposure to 325 °C. Inset photo shows the composite maintains stretchability.

Future work will include investigating the thermo-mechanical and thermo-electrical responses of FKM-based electrical conductors.

2.4. Printing of LM-FKM for Thermal Management

To use the enhanced material properties offered by LM composites and pattern the materials into functional structures, LM composite emulsion inks have been previously developed.[7,13,57–59] A variety of LM emulsion inks have been explored, including using matrix materials of silicones, including Sylgard, and aqueous solutions, including sodium carboxylmethyl cellulose. Prior studies have shown that by increasing the LM content in an emulsion ink, rheological properties can be improved for 3D printing.[13,53] Contents above 64% vol. are frequently used to achieve suitable rheology, including recent emulsion inks using 70% and 76.4% fill fractions.[13,53] Here, a LM-FKM emulsion ink is developed and demonstrated for printing of thermally stable structures. To create a printable ink of LM-Daikin, the polymer-to-solvent mass ratio was increased from 22.5% to 50% in order to form a polymer solution of higher viscosity. Following previous works, LM was added in a 75% volume fill fraction. **Figure 5**a shows the measured storage and loss modulus of the LM-FKM emulsion ink in comparison to the FKM-only ink. For a 3D printable ink, it is desired for the ink to be similar to a viscoelastic solid, where storage modulus is greater than loss modulus, at low frequencies and a viscoelastic liquid, where storage modulus is less than loss modulus, at high frequencies.[13,53] Low frequencies correspond to a printed trace after deposition while while high frequencies correspond to the flow of the ink through a printing nozzle. As shown in Figure 5a, an ink of only Daikin material behaves as a liquid at all tested frequencies, which suggests the material would continue to deform after printing and before drying. However, the addition of LM droplets creates an emulsion ink more suitable for printing where there exists a crossover in storage and loss modulus. At low frequencies the LM emulsion ink behaves as a solid while at high frequencies the LM emulsion ink behaves as a liquid. These results correspond well with previous reports of storage and loss modulus with LM composite emulsion inks, and the use of 75% volume fill fraction closely follows previous emulsion ink recipes.[13,53] Further optimization of the emulsion ink by adjusting both the LM and solvent content could shift the crossover in moduli to a higher frequency, and allow for an estimate of yield stress. The addition of LM also increases the apparent viscosity of the emulsion ink by two orders of magnitude (Figure 5b), which compares well with emulsion inks of high LM content.[13,53] Figure 5c displays an image of printing a third layer of a patterned trace with the thermally conductive and stable FKM. Printed traces are 1.3 mm wide when deposited

from a 22 G nozzle and can be used to create freestanding structures. While the emulsion ink developed here is printed with a direct ink writing method, there remains opportunity to further improve the emulsion ink composition and printing parameters to make it more compatible for 3D printing of soft structures. This includes further tuning the emulsion ink to demonstrate log-linear shear-thinning behaviors that are more suitable for fitting to a Herschel-Bulkley model and to determine a yield stress of the ink.[53,60] Additionally, since printing parameters and paths were not optimized within the scope of this work, there are remaining studies to be completed more specific to 3D printing of LM and FKM emulsion inks.

Owing to the high thermal stability of LM-FKM composites, the printable ink can be applied for structures in high-temperature settings, such as flexible heat sinks for thermal management, without mechanically degrading. Using the LM-FKM ink, flexible heat sinks with thin, parallel heat fins were 3D printed (Figure 5d; Figure S16, Supporting Information). Up to eight passes can be layered to achieve a heat fin with an aspect ratio of 3.5. The printed heat sink uses a set of five parallel heat fins to mimic common heat sink designs. To demonstrate thermal management, a 3D-printed LM-FKM heat sink was compared to a flat heat sink of Daikin, a flat heat sink of Daikin with 75% fill fraction of LM, and a commercial heat sink of similar size. The heat sinks were placed on a hot plate at a set temperature. Infrared images shown in Figure 5e confirmed the improvement in thermal dissipation over time offered by the 3D printed LM-FKM structure (Video S3, Supporting Information). Infrared images for all tested heat sinks are shown in Figure S17 (Supporting Information). Figure 5f displays the average temperature over the four heat sinks on a hot plate set to 135 °C. All heat sinks were characterized in a flat position for direct comparison to the commercial heat sink. The addition of LM significantly lowers the temperature of the surface, while the 3D printed structure offers enhanced thermal dissipation that is comparable to the commercially available heat sink. The comparable performance is a result of the design and size of the printed heat sink and the commercial heat sink. The printed heat sink is 20×20 mm[2] with a one-dimensional array of five heat fins. The commercial heat sink is 14×14 mm2 with a 2D array of 16 heat fins, each with a smaller-scale structure on their surface. The total surface area, including fins, of the printed heat sink and the commercial heat sink is 1400 mm2 and 940 mm[2 and this larger surface area enables the printed heat sink to offer a comparable performance to the more complexly detailed commercial heat sink. Figure 5g demonstrates the heat sinks performing at a lower temperature of 75 °C (additional data in Figure S18, Supporting Information). Overall, 3D printing with LM-FKM inks enables patterning of a soft, thermally structures and is capable of creating flexible heat sinks with similar performance to commercial heat sinks.

To highlight the thermo-mechanical stability of FKM in comparison to elastomer composites for high temperature applications, a patch of LM-Sylgard and LM-Viton were applied to a flexible steel film and heated to 325 °C for 10 min. After heating, the flexible steel films were immediately bent manually to apply a curved radius (>3 cm) to the thermally conductive materials. Figure 5h shows the LM-Sylgard forms cracks along the bending region, indicating thermo-mechanical instability and incompatibility with operation on flexible structures. However, the LM-Viton based composite maintains mechanical integrity and can even be peeled off the steel surface and stretched by hand without failure (Figure 5i). Overall, the ability to 3D print highly thermally conductive and stable soft material offers a means to fabricate a variety of high-temperature soft components.

2.5. Endoscopic Sensor for Wireless Temperature Sensing

To demonstrate the applicability of FKM-based materials for soft sensors and flexible robotics in high-temperature operation, a flexible endoscopic sensor was fabricated using Daikin and LM-Daikin as the outer encapsulation of a wirelessly connected temperature sensor. This demonstration highlights a potential use case of FKM-based composites for soft robotics in extreme environments. An illustration of the endoscopic sensor is shown in **Figure 6**a where a Bluetooth transmitter and thermocouple amplifier was packaged within a silicone shell and an outer FKM encapsulation. The tip of a thermocouple is embedded into a LM-FKM pathway, which served as a thermally conductive pathway to enable temperature sensing. The voltage generated from the thermocouple is amplified and sent via Bluetooth. The endoscopic sensor was manually moved from the distal end of the tubing. The endoscopic sensor was deployed on a surface of heated rocks (Figure 6b; Video S4, Supporting Information) to detect changes in temperature across the surface. Figure 6c shows a representative set of wirelessly transmitted temperature sensing as the endoscopic sensor is moved toward a strong heat source. Additionally, the endoscopic sensor was maneuvered across a set of three hotplates set to three different temperatures (Figure 6d). The shaded blue regions indicate areas between adjacent hotplates, while the yellow areas indicate the edge of the hotplate. Red areas mark the center of the hot plate. As shown by the wireless temperature sensing, the increases and decreases in temperature as the end of the endoscopic sensor is moved across these locations were captured.

3. Conclusion

In this work, soft, thermally stable LM composites are introduced with the use of FKMs as a polymer matrix material. LM-FKM composites maintain rubbery mechanical properties despite exposure to temperatures up to 325 °C, whereas LM-elastomer composites show mechanical degradation with increasing temperature. The properties of LM-FKM and LM-elastomer composites were evaluated across mechanical, thermal, and electrical properties to determine the effects of LM droplets on thermal stability. The thermo-mechanical responses displayed the advantages of using FKM as a matrix material for high thermal stability, while LM inclusions could offer means to toughen composites at high temperatures while providing enhanced thermal conductivity and dielectric constants. While embedding LM in Sylgard and Ecoflex offered a moderate improvement in thermo-mechanical stability, Vytaflex and SIS composites showed no improvements. In addition, electrically conductive LM-FKMs and printable LM-FKMs offered a promising approach to fabricating multi-material, fully FKM-based soft machines for operation in extreme environments.

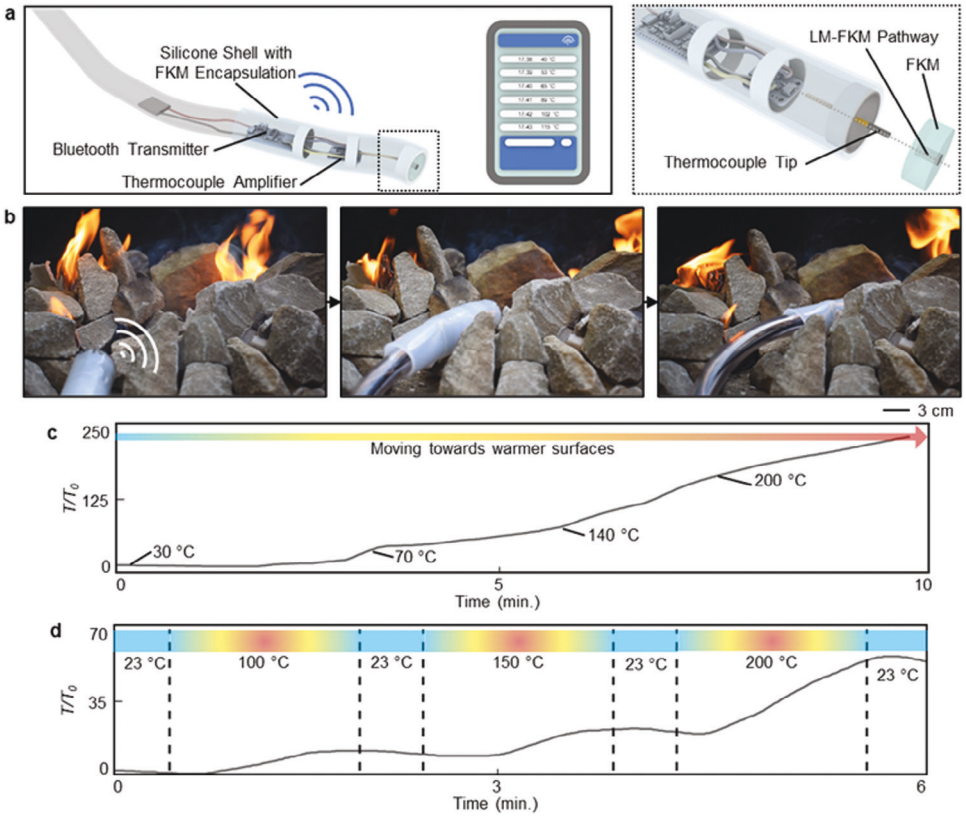

Figure 6. Endoscopic sensor for high temperature sensing. a) Schematic of flexible endoscopic sensor for wireless temperature sensing with exploded view of the thermocouple and LM-FKM interface. b) Images of endoscopic sensor traversing a surface of heat rocks. c) Wirelessly recorded temperature change over time as endoscope is moved closer to a strong heat source. d) Temperature changes recorded as endoscope is maneuvered across three hot plates set to 100, 150, and 200 °C.

While this work provides a comprehensive examination of the effect of LM on the material properties of FKMs and their thermal stability, future work is required to better understand the effects of process parameters, polymer solution viscosity, and LM droplet size, among additional parameters. Further work is also required elucidate reasons why LM effects on thermo-mechanical stability are variable among different FKM types and LM concentrations. Additionally, methods to test mechanical and dielectric Properties across a broad temperature range will provide insight into properties during exposure to high heat compared to the properties measured here after heat exposure.

The use of FKM as a matrix material has the potential to extend the use of LMEE composites in a wider range of applications. For example, printing of thermally conductive FKMs was demonstrated for thermal management and high-temperature exposure without mechanical degradation, which could be applied to an assortment of soft, thermally stable, and high-temperature components. An FKM-encapsulated endoscopic sensor displayed the potential for applying FKM-based soft robotics in high-temperature environments. Future use cases may include aerospace and in-space applications where materials are subject to wide temperature ranges. Collectively, these results provide insight into the effect of LM on the thermal stability of soft materials and the promising directions offered by LM-FKM composites, including for soft robotics in the extreme environments of high-temperature settings and space applications.

4. Experimental Section

Synthesis of LM Composites: FKMs were dissolved in DMF (Sigma–Aldrich) to create a 22.5% polymer solution. Tested FKMs included Viton (A401C, Chemours), Daikin (G801EL, Daikin), PVDF-HFP (Sigma–Aldrich; 427 160), PVDF (Sigma–Aldrich; 427 144), PVDF-CTFE (PolyK Technologies), and PVDF-CTFE-Trfe (PolyK Technologies). Mixing solvent and FKMs were performed on a hotplate set to 60 °C with a magnetic stirrer and occasional manual stirring until a uniform solution was achieved. Tested elastomers included Ecoflex (Ecoflex 30, Smooth-On), Sylgard (Sylgard 184, Dow Corning Corp), Vytaflex (Vytaflex 30, Smooth-On), and SIS. Prior to mixing Ecoflex, Sylgard, and Vytaflex with EGaIn, elastomer was diluted with toluene in a 20% mass ratio of elastomer to toluene. SIS was created by mixing SIS pellets (22.5 wt.% of styrene, Sigma–Aldrich; 432 415) with toluene to form a solution of 15% mass SIS. SIS was mixed on a hotplate set to 60 °C with a magnetic stirrer and occasional manual stirring until a uniform solution was achieved. Gallium and Indium (Rotometals Inc.) were mixed at 200 °C for 24 h in a 3:1 weight ratio to form EGaIn. EGaIn was added to the polymer solutions and mixed in a planetary centrifugal mixer (AR-100, Thinky Corp) for 3 min at 2000 RPM. Films were cast on glass slides coated with mold release and dried at 120 °C for 2 h in an oven. SIS composites were dried at room temperature for 1 h and then dried at 80 °C for 1 h. Ecoflex, Sylgard, and Vytaflex composites were cured

at 120 °C for 1 h. Electrically conductive Viton samples were prepared by mixing 1 g of polymer solution with 3 g of EGaIn and 1.2 g of Ag flakes (Sigma–Aldrich).

Microscopy Imaging: Optical images were taken with a confocal microscope (LSM 900, Zeiss) at 10x magnification with a numerical aperture of 0.4. SEM images were captured with a desktop SEM (Phenom XL) at a low vacuum of 60 Pa with a 15 kV beam.

Thermo-Mechanical Characterization: Tensile samples were cut from cast films into ≈0.2 mm x 3.5 mm x 15 mm strips. Measurements were performed on a materials testing tool (Instron 5969, Illinois Tool Works Inc) using a 50 N load cell and a strain rate of 1.5 mm s^{-1}. A 1 kN load cell was used for PVDF-HFP. For temperature exposures, samples were placed on a glass slide coated with mold release and placed onto the center of a pre-heated hotplate at the set temperature points for 10 min. A new set of samples was used at each temperature. A handheld infrared thermometer was used to verify hotplate surface temperature. After heating, samples were removed and cooled to room temperature prior to tensile testing. Samples for DMA testing were prepared in Teflon molds to create an ≈0.25 mm x 4 mm x 10 mm strip. An RSE-G2 Solids Analyzer (TA Instruments) was used. A strain rate of 5% s^{-1} was applied. Tensile modulus was measured based on 10% strain. For measurements of storage modulus, loss modulus, and damping factor, a heating rate of 5°C min^{-1} was used with a controlled strain of 1%. TGA was performed in an N_2 environment with sample masses of ≈10 mg.

Thermal Conductivity Measurement: Thermal conductivity was measured using a thermal interface material analyzer (TIMA 5, Nanotest). Samples were placed in solution form onto the sample plates of the tool. Thermal resistance was measured at bond line thicknesses of 200, 150, 100, 50, and 25 µm. The cold plate was set to 15.5 °C and the hot plate was set to 50 °C.

Electrical Properties: Samples were prepared by casting films onto stainless steel shim. After drying, EGaIn was dispensed into ≈3 mm diameters on top of the films to form a capacitor using the steel shim and EGaIn droplet as the electrodes. Capacitance was measured by connecting to the steel shim and using a wire probe to connect to the EGaIn droplet. Capacitance was measured with an LCR meter (889B, BK Precision) and measured with a frequency of 1 kHz and a bias of 1 V. Dielectric constant was calculated based on measured capacitance and thickness of the casted films. Dissipation factor was measured directly with an LCR meter. For temperature exposure, samples were measured and then placed on a pre-heated hot plate at the set temperature for 10 min. After heating, samples were removed and cooled to room temperature before measuring. Here, temperature exposure was consecutively tested (same set of samples tested at room temperature, 100, 175, 250, and 325 °C). Electrically conductive samples were measured with a handheld multimeter.

Rheological Measurements: Printable LM-FKM ink was created by mixing Daikin in a 1:1 mass ratio with DMF before adding 75% EGaIn by volume. An ink of FKM only was created by mixing Daikin in a 1:1 mass ratio with DMF. A rheometer (Discovery HR2, TA Instruments) was used to measure rheology of the inks. Measurements were taken with a 40 mm parallel plate configuration with a 0.8 mm gap height. Storage and loss moduli were measured at room temperature while sweeping angular frequency from 10^{-2} to 102 rad s^{-1}. Apparent viscosity was measured while sweeping shear rate from 10^{-2} to 102 s^{-1}.

3D Printing: 3D printing of LM-FKM ink was performed using a syringe extruder (SDS-5, Hyrel3D) and a 3D printer (System 30 M, Hyrel3D) with a tapered nozzle size of 22 G. A print speed of 2.5 mm s^{-1} was used with a layer height of 0.7 mm. Printable LM-FKM ink was created by mixing Daikin in a 1:1 mass ratio with DMF before adding 75% EGaIn by volume and mixing for 9 min.

Heat Sink Characterization: 3D heat sinks were printed as described above. Heat sink patches were fabricated by casting films on a glass slide and then laminating onto a steel surface. An infrared camera (AX35, FLIR) was used to capture thermal images, videos, and temperature data of the surfaces. FLIR data was captured with a hotplate set to various temperatures.

Endoscopic Sensor Fabrication and Temperature Sensing: An endoscopic sensor was fabricated using a flexible tubing guide with custom end attachment. The end attachment consisted of inner cylindrical supports, an inner silicone (Ecoflex 30, Smooth-On) shell, and an outer Daikin encapsulation. The end of the endoscope used a column of LM-Daikin for a thermally conductive pathway connected to the interior thermocouple. A Bluetooth temperature sensor was packaged inside the end of the endoscope. The sensor was created with a Bluetooth board (Adafruit Feather nRF52840 Express), a thermocouple amplifier (Adafruit MCP9600), and a Type K thermocouple (Adafruit). The voltage generated by the thermocouple is fed to the amplifier board before being transmitted via Bluetooth from the Feather board to a cellphone. A custom Arduino sketch was used to wirelessly transmit temperature data. Temperature values were sent via Bluetooth at a rate of 1 s^{-1}. The endoscopic sensor was manually manuevered from the distal end of the tubing. To simulate high-temperature conditions, a concrete pit was filled with 15 charcoal briquettes and lit. Pieces of cardboard were set among the rocks to generate more localized heat effects. A layer of rocks were placed over the charcoals and the endoscopic sensor was guided around the rocks and toward an area of highest temperature.

Supporting Information

Supporting Information is available from the Wiley Online Library or from the author.

Acknowledgements

R.H. and C.M. acknowledged support from the Space University Research Initiative (SURI) by the Air Force Research Laboratory (AFRL). K.M. and P.M. acknowledged support from NSF (DMR 2202747. PM acknowledged financial support from the Swiss National Science Foundation (SNSF, grant no. 194385). Y.Z. and M.R.B. acknowledged financial support by the National Science Foundation via DMR-2209587. The authors thank Dylan Shah and Toby Mea (Arieca, Inc.) for setting up thermal conductivity measurements.

Conflict of Interest

The authors declare no conflict of interest.

Data Availability Statement

The data that support the findings of this study are available in the supplementary material of this article.

Keywords

fluoroelastomers, high temperature, liquid metal composites, soft multifunctional materials, soft robotics, thermal stability

Received: August 15, 2023
Revised: November 13, 2023
Published online:

[1] C. Wang, C. Wang, Z. Huang, S. Xu, *Adv. Mater.* **2018**, *30*, 1801368.
[2] M. D. Bartlett, N. Kazem, M. J. Powell-Palm, X. Huang, W. Sun, J. A. Malen, C. Majidi, *Proc. Natl. Acad. Sci. USA* **2017**, *114*, 2143.
[3] R. Tutika, S. H. Zhou, R. E. Napolitano, M. D. Bartlett, *Adv. Funct. Mater.* **2018**, *28*, 1804336.
[4] G. G. Guymon, M. H. Malakooti, *J. Polymer Sci.* **2022**, *60*, 1300.

[5] S. Chen, H.-Z. Wang, T.-Y. Liu, J. Liu, *Adv. Intell. Syst.* **2023**, *5*, 2200375.
[6] Q. Shen, M. Jiang, R. Wang, K. Song, M. H. Vong, W. Jung, F. Krisnadi, R. Kan, F. Zheng, B. Fu, P. Tao, C. Song, G. Weng, B. Peng, J. Wang, W. Shang, M. D. Dickey, T. Deng, *Science* **2023**, *379*, 488.
[7] A. Haake, R. Tutika, G. M. Schloer, M. D. Bartlett, E. J. Markvicka, *Adv. Mater.* **2022**, *34*, 2200182.
[8] E. J. Markvicka, M. D. Bartlett, X. Huang, C. Majidi, *Nat. Mater.* **2018**, *17*, 618.
[9] M. D. Bartlett, A. Fassler, N. Kazem, E. J. Markvicka, P. Mandal, C. Majidi, *Adv. Mater.* **2016**, *28*, 3726.
[10] N. Kazem, M. D. Bartlett, C. Majidi, *Adv. Mater.* **2018**, *30*, 1706594.
[11] A. Hajalilou, A. F. Silva, P. A. Lopes, E. Parvini, C. Majidi, M. Tavakoli, *Adv. Mater. Interfaces* **2022**, *9*, 2101913.
[12] M. R. Vinciguerra, D. K. Patel, W. Zu, M. Tavakoli, C. Majidi, L. Yao, *ACS Appl. Mater. Interfaces* **2023**, *15*, 24777.
[13] P. Won, C. S. Valentine, M. Zadan, C. Pan, M. Vinciguerra, D. K. Patel, S. H. Ko, L. M. Walker, C. Majidi, *ACS Appl. Mater. Interfaces* **2022**, *14*, 55028.
[14] C. Majidi, K. Alizadeh, Y. Ohm, A. Silva, M. Tavakoli, *Flexible Printed Electron.* **2022**, *7*, 013002.
[15] Y. Han, L.-E. Simonsen, M. H. Malakooti, *Adv. Energy Materials* **2022**, *12*, 2201413.
[16] M. Zadan, M. H. Malakooti, C. Majidi, *ACS Appl. Mater. interfaces* **2020**, *12*, 17921.
[17] N. Kazem, T. Hellebrekers, C. Majidi, *Adv. Mater.* **2017**, *29*, 1605985.
[18] M. D. Dickey, R. C. Chiechi, R. J. Larsen, E. A. Weiss, D. A. Weitz, G. M. Whitesides, *Adv. Funct. Mater.* **2008**, *18*, 1097.
[19] X. Li, M. Li, L. Zong, X. Wu, J. You, P. Du, C. Li, *Adv. Funct. Mater.* **2018**, *28*, 1804197.
[20] J.-H. Kim, S. Kim, J.-H. So, K. Kim, H.-J. Koo, *ACS Appl. Mater. Interfaces* **2018**, *10*, 17448.
[21] P. Won, S. Coyle, S. H. Ko, D. Quinn, K. J. Hsia, P. Leduc, C. Majidi, *Adv. Healthcare Mater.* **2023**, 2202430.
[22] G.-H. Lee, H. Woo, C. Yoon, C. Yang, J.-Y. Bae, W. Kim, D. H. Lee, H. Kang, S. Han, S.-K. Kang, S. Park, H.-R. Kim, J.-W. Jeong, S. Park, *Adv. Mater.* **2022**, *34*, 2204159.
[23] S. Chen, R. Zhao, X. Sun, H. Wang, L. Li, J. Liu, *Adv. Healthcare Mater.* **2023**, *12*, 2201924.
[24] C. Pan, E. J. Markvicka, M. H. Malakooti, J. Yan, L. Hu, K. Matyjaszewski, C. Majidi, *Adv. Mater.* **2019**, *31*, 1900663.
[25] Y. Wang, Z. Yu, G. Mao, Y. Liu, G. Liu, J. Shang, S. Qu, Q. Chen, R.-W. Li, *Adv. Mater. Technol.* **2019**, *4*, 1800435.
[26] M. H. Malakooti, N. Kazem, J. Yan, C. Pan, E. J. Markvicka, K. Matyjaszewski, C. Majidi, *Adv. funct. mater.* **2019**, *29*, 1906098.
[27] M. J. Ford, D. K. Patel, C. Pan, S. Bergbreiter, C. Majidi, *Adv. Mater.* **2020**, *32*, 2002929.
[28] A. Mitra, K. Xu, S. Babu, J. H. Choi, J.-B. Lee, *Adv. Mater. Interfaces* **2022**, *9*, 2102141.
[29] W. Zu, Y. Ohm, M. R. Carneiro, M. Vinciguerra, M. Tavakoli, C. Majidi, *Adv. Mater. Techn.* **2022**, *7*, 2200534.
[30] R. Tutika, A. B. M. T. Haque, M. D. Bartlett, *Commun. Mater.* **2021**, *2*, 64.
[31] Y. Li, S. Feng, S. Cao, J. Zhang, D. Kong, *ACS Appl. Mater. Interfaces* **2020**, *12*, 50852.
[32] A. B. M. T. Haque, R. Tutika, R. L. Byrum, M. D. Bartlett, *Adv. Funct. Mater.* **2020**, *30*, 2000832.
[33] M. Reis Carneiro, C. Majidi, M. Tavakoli, *Adv. Funct. Mater.* **2022**, *32*, 2205956.
[34] Y. Zhang, P. Li, J. Quan, L. Li, G. Zhang, D. Zhou, *Adv. Intell. Syst.* **2023**, *5*, 2200071.
[35] T. TolleyMichael, F. ShepherdRobert, C. GallowayKevin, J. WoodRobert, M. WhitesidesGeorge, *Soft robotics* **2014**, *1*, 213.
[36] L. Jing, L.-Y. Hsiao, S. Li, H. Yang, P. L. P. Ng, M. Ding, T. V. Truong, S.-P. Gao, K. Li, Y.-X. Guo, P. Valdivia Y Alvarado, P.-Y. Chen, *Mater. Horiz.* **2021**, *8*, 2065.
[37] H. Wang, W. Xing, S. Chen, C. Song, M. D. Dickey, T. Deng, *Adv. Mater.* **2021**, *33*, 2103104.
[38] L.-C. Jia, Y.-F. Jin, J.-W. Ren, L.-H. Zhao, D.-X. Yan, Z.-M. Li, *J. Mater. Chem. C* **2021**, *9*, 2904.
[39] H. Jin, M. O. G. Nayeem, S. Lee, N. Matsuhisa, D. Inoue, T. Yokota, D. Hashizume, T. Someya, *ACS Nano* **2019**, *13*, 7905.
[40] T. Sekitani, Y. Noguchi, K. Hata, T. Fukushima, T. Aida, T. Someya, *Science* **2008**, *321*, 1468.
[41] Q. Li, C. Ding, W. Yuan, R. Xie, X. Zhou, Y. Zhao, M. Yu, Z. Yang, J. Sun, Q. Tian, F. Han, H. Li, X. Deng, G. Li, Z. Liu, *Adv. Fiber Mater.* **2021**, *3*, 302.
[42] H. Jin, N. Matsuhisa, S. Lee, M. Abbas, T. Yokota, T. Someya, *Adv. Mater.* **2017**, *29*, 1605848.
[43] D. Berthier, M.-P. Deffarges, N. Berton, M. Venin, F. Lacroix, B. Schmaltz, Y. Tendron, E. Pestel, F. Tran-Van, S. Méo, *Materials* **2018**, *11*, 1358.
[44] J. Heidarian, A. Hassan, *Composites, Part B* **2014**, *58*, 166.
[45] J. Zhang, Q. Lu, Y. Li, T. Li, M.-H. Lu, Y.-F. Chen, D. Kong, *ACS Mater. Letters* **2021**, *3*, 1104.
[46] T. Sekitani, H. Nakajima, H. Maeda, T. Fukushima, T. Aida, K. Hata, T. Someya, *Nat. Mater.* **2009**, *8*, 494.
[47] L. Zheng, M. Zhu, B. Wu, Z. Li, S. Sun, P. Wu, *Sci. adv.* **2021**, *7*, eabg4041.
[48] M. J. Ford, M. Palaniswamy, C. P. Ambulo, T. H. Ware, C. Majidi, *Soft Matter* **2020**, *16*, 5878.
[49] W. Song, V. L. Tagarielli, K.-Y. Lee, *Macromol. Mater. Eng.* **2018**, *303*, 1800363.
[50] J.-B. Bao, T. Liu, L. Zhao, G.-H. Hu, X. Miao, X. Li, *Polymer* **2012**, *53*, 5982.
[51] X. Zhi, H.-B. Zhang, Y.-F. Liao, Q.-H. Hu, C.-X. Gui, Z.-Z. Yu, *Carbon* **2015**, *82*, 195.
[52] S. He, D. Carolan, A. Fergusson, A. C. Taylor, *Mater. Des.* **2019**, *169*, 107654.
[53] J. D. Eshelby, *Proc. R. Soc. London, Ser. A* **1957**, *241*, 376.
[54] Y. Hu, C. Majidi, *ACS Appl. Mater. Interfaces* **2023**.
[55] D. K. Rana, P. S. Banerjee, S. S. Banerjee, *J. Mater. Sci.* **2023**, *58*, 6375.
[56] H. C. Nguyen, V. T. Doan, J. Park, J. C. Koo, Y. Lee, J.-D. Nam, H. R. Choi, *Smart Mater. Struct.* **2008**, *18*, 015006.
[57] R. E. Sánchez Cruz, S. F. Zopf, J. W. Boley, *J. Compos. Mater.* **2023**, *57*, 829.
[58] Q. Wang, X. Ji, X. Liu, Y. Liu, J. Liang, *ACS Nano* **2022**, *16*, 12677.
[59] L. Y. Zhou, J. Z. Fu, Q. Gao, P. Zhao, Y. He, *Adv. Funct. Mater.* **2020**, *30*, 1906683.
[60] W. H. Herschel, R. Bulkley, *Kolloid-Zeit* **1926**, *39*, 291.